Accurate computation of laminar boundary-layer flows using a residual-based scheme

Christophe Eric Corre, G. Hanss, Eric Goncalvès da Silva

Accurate computation of laminar boundary-layer flows using a residual-based scheme

C. Corre, G. Hanss and E. Goncalves

SINUMEF Laboratory - ENSAM
151, Bd de l'Hopital, 75013 Paris, France
corre@paris.ensam.fr

1. Introduction

The calculation of viscous compressible flows makes routine use of discretization schemes which are numerically dissipative. This numerical dissipation, usually tailored within the framework of the Euler equations, is likely to affect the global accuracy of the solution when applied to a viscous problem : such a contamination of a laminar boundary layer by scalar artifical dissipation was pointed out for instance by Allmaras in [1]. In the same work, Allmaras observed that matrix dissipation allowed a large improvement of the velocity profile prediction, even on rather coarse grids, thanks to a better scaled dissipation; this result was later confirmed in [2]. In the present work, an original scheme with residual-based dissipation, first introduced in [3] to solve the compressible Navier-Stokes equations, is compared with standard scalar and matrix dissipation schemes in order to assess its accuracy properties. The computation of a flat-plate boundary layer flow as well as a viscous flow with pressure gradient and the careful analysis of the results allow to conclude that the residual-based scheme yields very accurate velocity and temperature profiles even on extremely coarse grids.

2. Description of the numerical methods

Consider the two-dimensional Navier-Stokes equations written in conservative form :

$$w_t + (f^E(w) - f^V(w, w_x, w_y))_x + (g^E(w) - g^V(w, w_x, w_y))_y = 0 \tag{1}$$

where t is the time, x and y are space coordinates, $w = w(x, y, t)$ is the state vector, f^E, g^E are the inviscid flux vector functions and f^V, g^V are the viscous flux vector functions. Let $v_{j,k}$ be a mesh function defined on a uniform Cartesian mesh ($x_j = j\,\delta x, y_k = k\,\delta y$), with steps δx and δy of order $O(h)$ and let us define the basic difference and average operators :

$$(\delta_1 v)_{j+\frac{1}{2},k} = v_{j+1,k} - v_{j,k} \qquad (\delta_2 v)_{j,k+\frac{1}{2}} = v_{j,k+1} - v_{j,k}$$
$$(\mu_1 v)_{j+\frac{1}{2},k} = \tfrac{1}{2}(v_{j+1,k} + v_{j,k}) \qquad (\mu_2 v)_{j,k+\frac{1}{2}} = \tfrac{1}{2}(v_{j,k+1} + v_{j,k}).$$

For the sake of clarity in the description of the numerical methods, let us assume in a first step that the viscous fluxes are zero so that (1) reduces to the Euler system of equations. It can be approximated using a conservative semi-discrete scheme written in this case as :

$$(w_t + \frac{\delta_1 F}{\delta x} + \frac{\delta_2 G}{\delta y})_{j,k} = 0 \tag{2}$$

with the numerical fluxes given for a large class of schemes by :

$$F_{j+\frac{1}{2},k} = (\tilde{F} - d_1)_{j+\frac{1}{2},k}\ ,\ \ G_{j,k+\frac{1}{2}} = (\tilde{G} - d_2)_{j,k+\frac{1}{2}} \tag{3}$$

where $\tilde{F}$, $\tilde{G}$ denote centered fluxes approximating respectively f^E and g^E while d_1, d_2 are numerical dissipation fluxes. The inviscid fluxes are classically discretized with second-order accuracy using simple centered differences :

$$\tilde{F} = \mu_1 f^E \ , \ \tilde{G} = \mu_2 g^E. \tag{4}$$

which lead to a truncation error of the form $\epsilon = \frac{\delta x^2}{6} f_{xxx} + \frac{\delta y^2}{6} g_{yyy} + O(h^4)$. The second-order error terms can be cancelled using third-order differences in each space direction; the following expressions :

$$\tilde{F} = \mu_1 (Id - \frac{\delta_1^2}{6}) f^E \ , \ \tilde{G} = \mu_2 (Id - \frac{\delta_2^2}{6}) g^E \tag{5}$$

lead to a fourth-order non-dissipative approximation of the Euler equations ($\epsilon = O(h^4)$). Alternatively, fourth-order accuracy can be obtained in a compact way using the fact the residual $r = f_x^E + g_y^E$ vanishes at steady-state [3]. It is easy to check the following non-dissipative approximations :

$$\tilde{F} = \mu_1 (Id + \frac{\delta_2^2}{6}) f^E \ , \ \tilde{G} = \mu_2 (Id + \frac{\delta_1^2}{6}) g^E \tag{6}$$

yield a truncation error of the form $\epsilon = r + \frac{1}{6}\delta x^2 r_{xx} + \frac{1}{6}\delta y^2 r_{yy} + O(h^4)$ and since $r = 0$ at steady-state, $\epsilon = O(h^4)$. For compressible flow calcnlations, approximations (4), (5) or (6) cannot be used as such and need to be completed with numerical dissipation. Three choices are considered in the present work, namely a high-order either scalar or matrix dissipation leading respectively to the well-known Jameson [4] and Roe-MUSCL [6]-[7] schemes, and an original residual-based dissipation [3]. The scalar dissipation of the Jameson scheme is scaled by the spectral radii ρ_A, ρ_B of the inviscid flux Jacobians $A = df^E/dw$ and $B = dg^E/dw$; more precisely :

$$d_1 = -k^{(4)} \overline{\rho}_A \delta_1^3 w \quad , \quad d_2 = -k^{(4)} \overline{\rho}_B \delta_2^3 w \tag{7}$$

where $k^{(4)}$ is a tunable coefficient and $\overline{\rho}_A$, $\overline{\rho}_B$ are modified expressions of the spectral radii including the correction proposed by Martinelli [5] to reduce the numerical dissipation on highly stretched grids. The matrix dissipation scheme is defined by :

$$d_1 = -\frac{1}{12} |A_R| \delta_1^3 w \quad , \quad d_2 = -\frac{1}{12} |B_R| \delta_2^3 w \tag{8}$$

where A_R (resp. B_R) denotes the Roe average [7] of the Jacobian A (resp. B). The third-order error introduced by both scalar and matrix dissipation terms can be written in the form $\epsilon^d = \delta x^3 (D_1 w_{3x})_x + \delta y^3 (D_2 w_{3y})_y$. The residual-based dissipation differs strongly from the previous choices since it is based on a low-order term which becomes third-order at steady-state, when r vanishes; it is given by :

$$d_1 = \frac{\delta x}{2} \Phi_1 (\frac{\delta_1 f^E}{\delta x} + \frac{\delta_2 \mu_1 \mu_2 g^E}{\delta y}) \ , \ d_2 = \frac{\delta y}{2} \Phi_2 (\frac{\delta_1 \mu_1 \mu_2 f^E}{\delta x} + \frac{\delta_2 g^E}{\delta y}) \tag{9}$$

where Φ_2, Φ_2 are matrix coefficients depending on the inviscid Jacobians eigenvalues which are designed to ensure the scheme dissipation (see [3] for more details). It is easy to check that the error introduced by the residual-based dissipation reads $\epsilon^d = \frac{\delta x}{2} (\Phi_1 r)_x + \frac{\delta y}{2} (\Phi_2 r)_y + O(h^3)$ and becomes third-order at steady-state where $r = 0$.

Let us now consider the full Navier-Stokes equations (1) and detail how the previous methods extend to the viscous case. The centered fluxes $\tilde{F}$ and $\tilde{G}$ approximate respectively $f^E - f^V$ and $g^E - g^V$ so that the formulae (4) become :

$$\tilde{F} = \mu_1 f^E - \tilde{f}^V \ , \ \tilde{G} = \mu_2 g^E - \tilde{g}^V \tag{10}$$

with $\tilde{f}^V = f^V(\mu_1 w, \frac{\delta_1 w}{\delta x}, \frac{\delta_2 \mu_1 \mu_2 w}{\delta y})$ and $\tilde{g}^V = g^V(\mu_2 w, \frac{\delta_1 \mu_1 \mu_2 w}{\delta x}, \frac{\delta_2 w}{\delta y})$. Using directional corrections to cancel the second-order error terms in (10) would considerably increase the scheme stencil because of the high-order derivatives introduced by the viscous fluxes; for practical applications, the following simplified high-order approximations are used :

$$\tilde{F} = \mu_1(Id - \frac{\delta_1^2}{6}) f^E - \tilde{f}^V \ , \ \tilde{G} = \mu_2(Id - \frac{\delta_2^2}{6}) g^E - \tilde{g}^V \tag{11}$$

which yield a second-order scheme in the general case since the viscous fluxes centered discretization is unchanged but lead to a fourth-order approximation of the Euler equations governing the flow outside the boundary layer. A truly fourth-order compact approximation of the Navier-Stokes equations was derived in [3] using the residual-based idea, with the residual now defined by $r = (f^E - f^V)_x + (g^E - g^V)_y$. In the present work, a simplified version is used because it was observed on the applications presented in the next section that a high-order approximation of the inviscid flow region only was sufficient to improve the prediction of boundary layer flow with pressure gradients; thus the residual-based high-order discretizations of $f^E - f^V$ and $g^E - g^V$ read :

$$\tilde{F} = \mu_1(Id + \frac{\delta_2^2}{6}) f^E - \tilde{f}^V \ , \ \tilde{G} = \mu_2(Id + \frac{\delta_1^2}{6}) g^E - \tilde{g}^V \tag{12}$$

and yield a fourth-order approximation of the Euler equations but are only second-order inside the boundary-layer. The scalar and matrix third-order dissipation (7), (8) remain unchanged for viscous problems while the residual-based dissipation is modified to take into account the viscous fluxes in the residual; the residual-based dissipative fluxes read :

$$d_1 = \frac{\delta x}{2}\Phi_1(\frac{\delta_1(f^E - \mu_1 \tilde{f}^V)}{\delta x} + \frac{\delta_2(\mu_1\mu_2 g^E - \mu_1 \tilde{g}^V)}{\delta y}) \ , \ d_2 = \frac{\delta y}{2}\Phi_2(\frac{\delta_1(\mu_1\mu_2 f^E - \mu_2 \tilde{f}^V)}{\delta x} + \frac{\delta_2(g^E - \mu_2 \tilde{g}^V)}{\delta y}) \tag{13}$$

and yield a third-order error at steady-state - Φ_1 and Φ_2 are unchanged with respect to the inviscid case -. From now on, the second-order schemes built using (2)-(10) with the dissipation flux formula (7), (8) or (13) will be denoted respectively SD, MD and RB (scalar, matrix or residual-based dissipation). The scheme defined by the directional correction (11) and matrix dissipation (8) will be denoted $MD(3)$ to indicate it is third-order outside the boundary-layer, while the approximation based on the residual-based correction (12) and dissipation (13) will be referred to as $RB(3)$. None of the schemes makes use of a limiter function.

3. Application to boundary-layer flows

Supersonic laminar flow over a flat-plate Schemes SD, MD and RB are now applied to the computation of the laminar flow over a flat-plate at $M = 2$ and $Re = 100000$ per unit length. The supersonic regime is considered because the solution is much less dependent on the proper choice of inlet and outlet boundary conditions than in the subsonic case, which allows to focus on the comparison of space discretizations. Note that the coefficient $k^{(4)}$ for SD is taken equal to 0.008; MD and RB are parameter free. The computational domain extends along the $x-$axis from $x = 0$ where all the free-stream values are imposed (supersonic inlet) up to $x = 4$ where the conserved quantities are extrapolated at first-order from the values at the nearest upstream location (supersonic ontlet) and along the $y-$axis from $y = 0$, where adiabatic wall conditions are prescribed, up to $y = 0.16$ treated as a supersonic outlet. The upper boundary is located at about 4 times the boundary layer thickness at station $x = 4$. Three grids are used in the computations, each containing 120 points uniformly distributed along the $x-$axis : the fine (resp. medium and coarse) grid contains 80 (resp. 40 and 20) points in the direction normal to

the plate, with a mesh spacing at the wall Δy_w equal to 5×10^{-4} (resp. 2×10^{-3}, 8×10^{-3}) which yields about 42 (resp. 16, 5) points within the boundary layer at the exit station.
The longitudinal velocity and temperature profiles computed at station $x = 3$ are displayed in Fig. 1 and 2 versus the boundary layer coordinate $\eta = y\sqrt{Re_x}/x$. On the fine grid, the 3 schemes yield velocity profiles in good agreement with the reference solution obtained using a boundary-layer code, though SD is less accurate than MD or RB; however, with 42 points in the boundary layer, SD is unable to predict the correct wall temperature while both MD and RB yield values very close to the recovery temperature. When using the medium grid, MD and RB solutions remain almost unchanged while the SD solution deviates strongly from the fine grid solution. On the coarse grid, the SD prediction becomes meaningless; MD could not be successfully converged to steady-state on this grid while RB is still able to provide an accurate solution with no more than 5 points in the boundary layer. Using $MD(3)$ (resp. $RB(3)$) instead of MD (resp. RB) yields very similar results.

Subsonic laminar flow over a NACA0012 airfoil The flow at $M_\infty = 0.5$ and $Re = 5000$ over a thermally insulated NACA0012 airfoil at zero incidence is computed using three C-meshes containing the same number of points (128×83) - only the upper part of the airfoil is considered owing to the problem symmetry - but with different mesh spacing at the wall varying from 1.2×10^{-2} for the coarse grid down to 4.8×10^{-3} and 4.8×10^{-4} respectively for the medium and fine grids. The main flow feature is a separation region occuring near the airfoil trailing edge caused by the adverse pressure gradient starting at about 10% of the chord. SD, with $k^{(4)}$ set equal to 0.016 for this problem and the second or third-order versions of MD and RB yield very similar results on the fine grid (see Table 1 below where the computed drag coefficients and separation location are summarized). However, the much higher sensitivity of SD to grid coarsening is observed again, as can be seen on the skin-friction distribution plotted in Fig. 3. The skin-friction peak located near the leading edge rapidly decreases with SD while the separation point, identified as the point where skin-friction becomes zero, is strongly shifted towards the leading edge on the medium grid; the flow computed with SD is fully attached on the coarse grid. Meanwhile, both second-order MD and RB preserve rather well the solution accuracy on the medium grid but fail to do so on the coarse grid : the skin-friction distribution strongly deviates from the fine and medium grid solution with a separation point located at about $x_s = 0.7c$. Using $MD(3)$ does not improve the prediction (see Fig.4) whereas using $RB(3)$ allows to obtain an accurate solution even on the coarse grid, with no shift in the separation location. The especially low sensitivity of this latter method is also made visible on the pressure coefficient distribution in Fig.5.

	SD			$MD(3)$			$RB(3)$		
	CD_f	CD_p	x_s	CD_f	CD_p	x_s	CD_f	CD_p	x_s
Fine grid	0.0328	0.0226	0.808	0.0327	0.0228	0.810	0.0326	0.0230	0.800
Medium grid	0.0325	0.0301	0.59	0.0303	0.0245	0.810	0.0320	0.0223	0.800
Coarse grid	0.0481	0.0171	×	0.0241	0.0305	0.67	0.0312	0.0208	0.800

Table 1: Laminar flow over an airfoil. Viscous and inviscid drag coefficients and separation location (chord %).

References

[1] S.R. Allmaras, "Contamination of laminar boundary-layers by artificial dissipation in Navier-Stokes solutions", *Proceedings of the Conference on Numerical Methods in Fluid Dynamics*, 443-449, Reading, England, UK (1992).

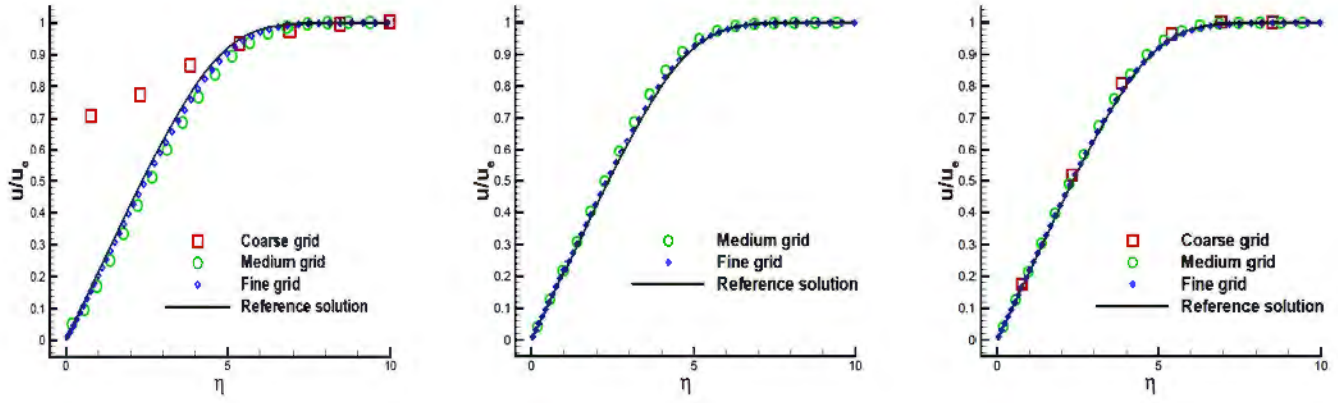

Figure 1: Laminar boundary layer over a flat plate. Effect of grid coarsening on the u-velocity profile at station $x = 3$ for the different schemes used. Left : SD; center : MD; right : RB.

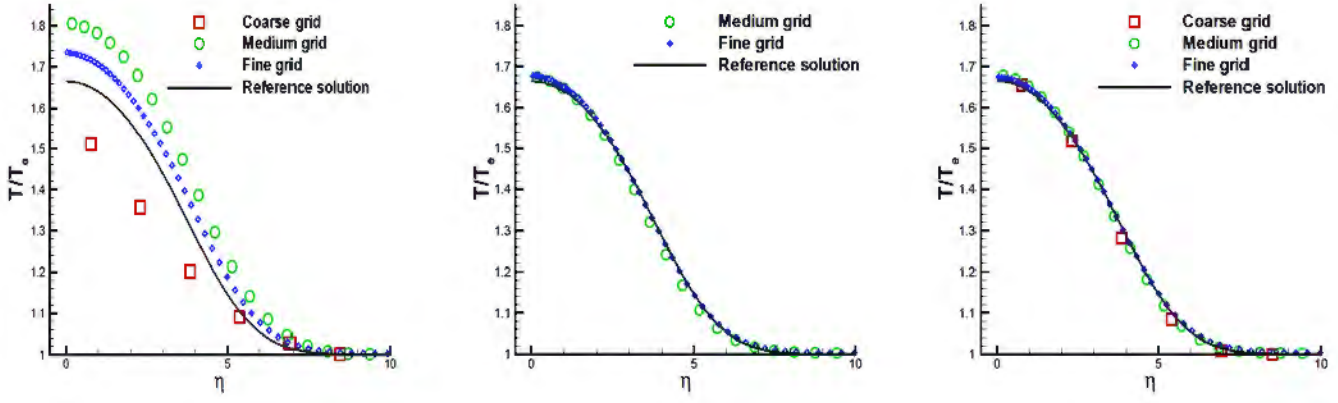

Figure 2: Laminar boundary layer over a flat plate. Effect of grid coarsening on the temperature profile at station $x = 3$ for the different schemes used. Left : SD; center : MD; right : RB.

[2] S. Tatsumi, L. Martinelli and A. Jameson, "Flux-Limited Schemes for the Compressible Navier-Stokes Equations", *AIAA J.*, **33**, No. 2, 252-261 (1995).

[3] A. Lerat and C. Corre, "A Residual-Based Compact Scheme for the Compressible Navier-Stokes Equations", *Journal of Computational Physics*, **170**, 642-675 (2001).

[4] A. Jameson, W. Schmidt and E. Turkel, "Numerical Solutions of the Euler Equations by Finite Volume Methods with Runge-Kutta Time Stepping Schemes", AIAA Paper 81-1259 (1981).

[5] L. Martinelli and A. Jameson, "Validation of a Multigrid Method for the Reynolds Averaged Equations", AIAA Paper 88-0414 (1988).

[6] B. Van Leer, "Towards the ultimate conservative difference scheme. V. A second-order sequel to Godunov's method", *Journal of Computational Physics*, **32**, 101-136 (1979).

[7] P.L. Roe, "Approximate Riemann solvers, parameter vectors and difference schemes", *Journal of Computational Physics*, **43**, 357-372 (1981).

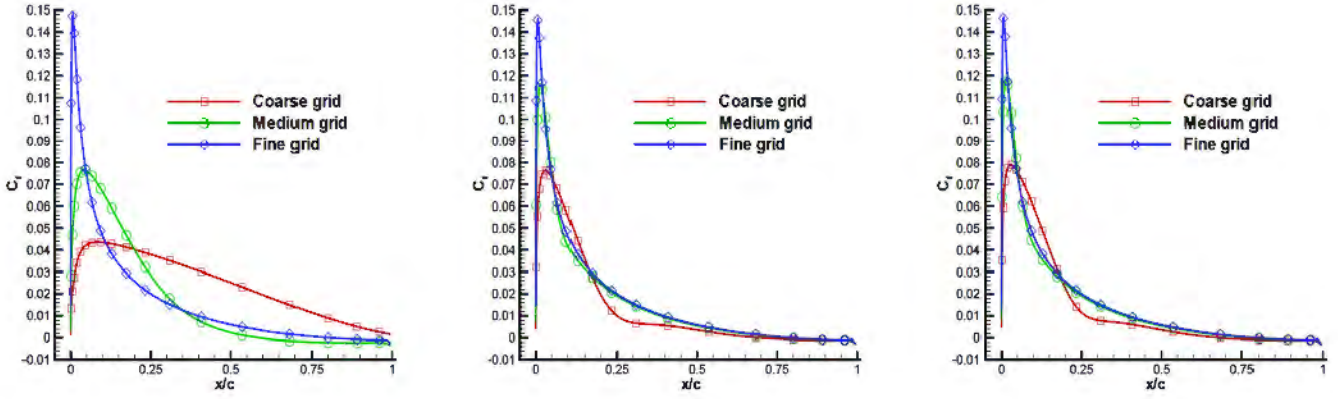

Figure 3: Laminar flow over an airfoil. Effect of grid-coarsening on the skin-friction coefficient distribution. Left : SD; center : MD; right : RB. *Only* 1 *out of* 5 *points is shown along the airfoil for the sake of clarity.*

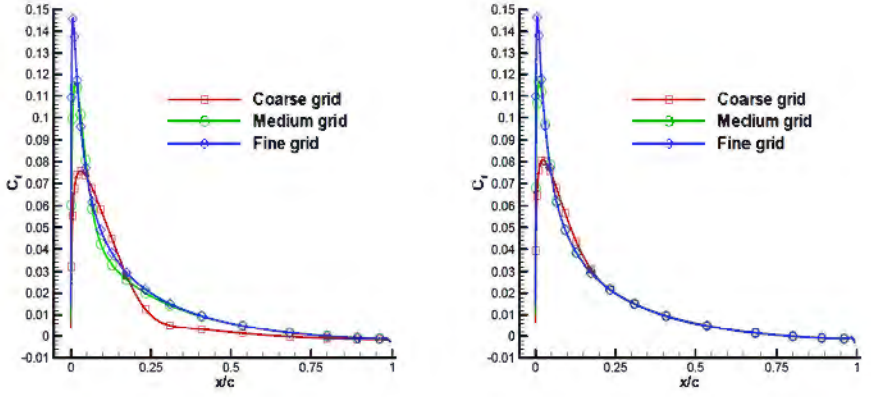

Figure 4: Laminar flow over an airfoil. Effect of grid-coarsening on the skin-friction coefficient distribution. Left : $MD(3)$; right : $RB(3)$.

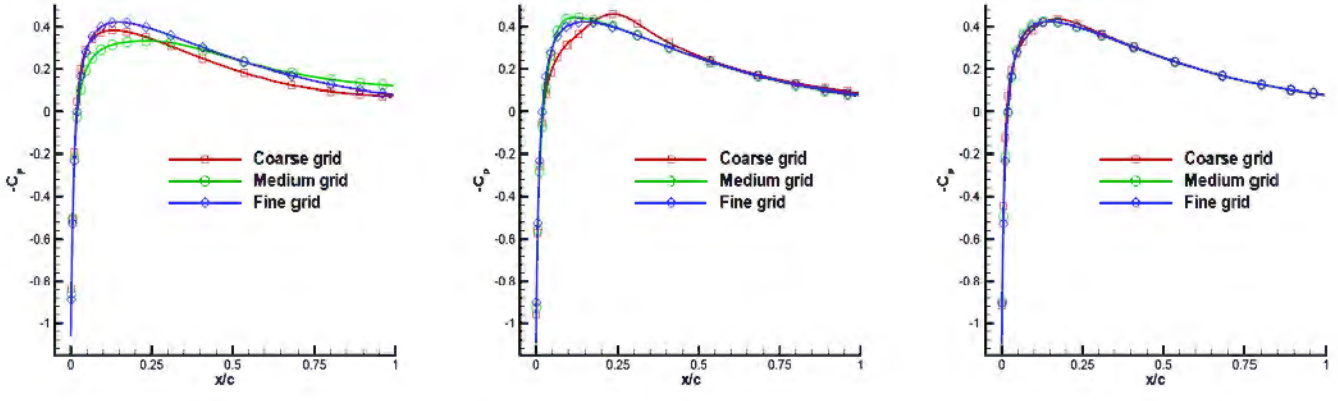

Figure 5: Laminar flow over an airfoil. Effect of grid-coarsening on the pressure coefficient distribution. Left : SD; center : $MD(3)$; right : $RB(3)$.